nature astronomy

Article

https://doi.org/10.1038/s41550-024-02271-2

Detection of an Earth-sized exoplanet orbiting the nearby ultracool dwarf star SPECULOOS-3

In the format provided by the authors and unedited

Detection of an Earth-sized exoplanet orbiting the nearby ultracool dwarf star SPECULOOS-3: Supplementary Information

Source Data Files Inventory

- Figure 1: Gillon_SPECULOOS3_SourceData_Fig1.csv
- Figure 2: Gillon_SPECULOOS3_SourceData_Fig2.csv
- Figure 3: Gillon_SPECULOOS3_SourceData_Fig3.csv
- Figure 4: Gillon_SPECULOOS3_SourceData_Fig4.csv
- Figure 5: Gillon_SPECULOOS3_SourceData_Fig5.csv
- Extended Data Figure 2: Gillon_SPECULOOS3_SourceData_ED_Fig2.csv
- Extended Data Figure 3: Gillon_SPECULOOS3_SourceData_ED_Fig3.csv
- Extended Data Figure 4: Gillon_SPECULOOS3_SourceData_ED_Fig4.csv

Data Repository

The ground-based and TESS light curves and the spectra used in this work are publicly available on the following online repository: https://doi.org/10.5281/zenodo.10821723

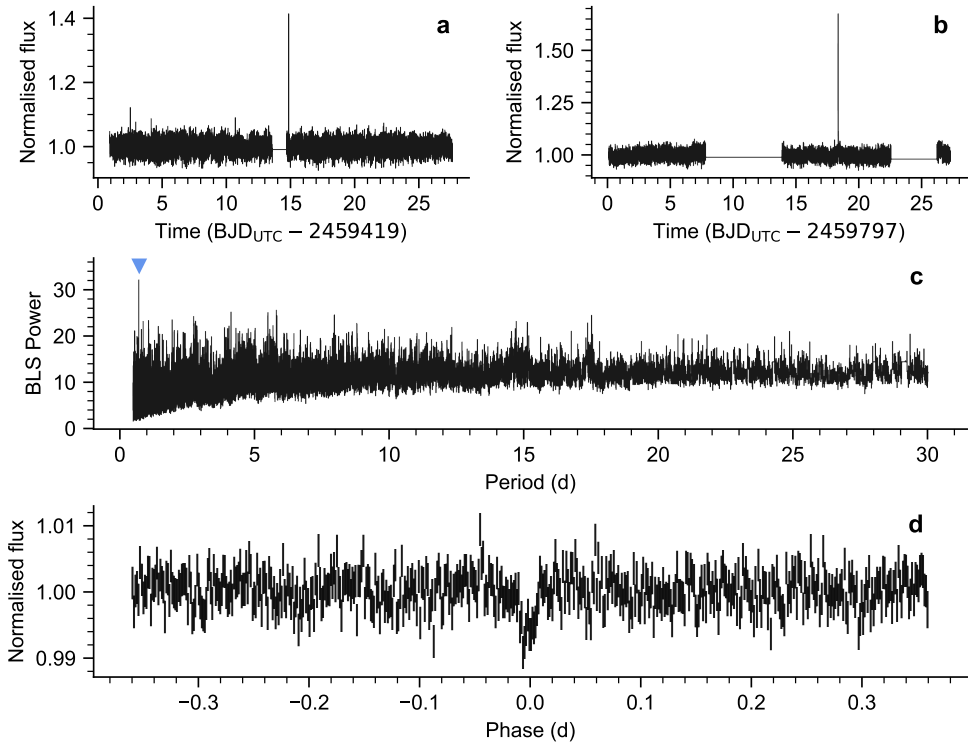

Supplementary Information Fig. 1 | TESS photometry of SPECULOOS-3. TESS Sector 41 and 55 light curves of SPECULOOS-3. The Sector 41 (**a**) and Sector 55 (**b**) TESS PDCSAP light curves of SPECULOOS-3 clearly show large flares (attributable to SPECULOOS-3) and complex variability (attributable to the nearby star TYC 2691-574-1). (**c**) After flattening the Sector 41+55 light curve, a box-least-squares analysis reveals a clear peak at the period of SPECULOOS-3 b, indicated by a blue triangle here. (**d**) The transit of SPECULOOS-3 b is evident after folding the light curve on this period and binning the data in 2-min bins.

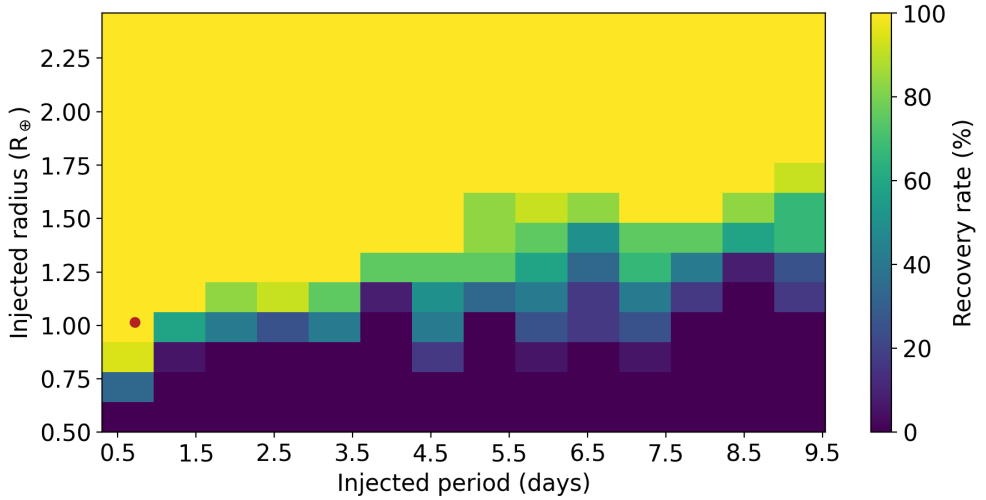

Supplementary Information Fig. 2 | Detectability of a second planet from TESS data. The injection-and-recovery experiment was conducted to test the detectability of transiting planets using the flattened TESS data from Sectors 41 and 55. We explored a total of 2700 different scenarios, that is, different combinations of planetary radius, orbital period, and phase. Each pixel represents about evaluated 20 scenarios. Higher recovery rates are presented in yellow and green colors, while lower recovery rates are shown in blue and darker hues. This experiment shows that Earth-size or smaller planets can only be detected for short orbital periods of $\leq$1 d in the current dataset. Transiting super-Earths with sizes larger than $\sim$1.5 $R_\oplus$ would be easily detected for the complete set of orbital periods explored in this study, allowing us to discard the existence of such planets in the system. The red dot corresponds to SPECULOOS-3 b.

Filter	Observatory	Date	Baseline	Comment
$I+z$	SAINT-EX	2021.07.27*	$p(t^2)$	
$I+z$	SAINT-EX	2021.07.29*	$p(t^2)$	
$I+z$	SNO-Artemis	2022.07.29	$p(t^3)$	flare
$I+z$	SNO-Artemis	2023.07.23	$p(t)$	
$I+z$	SNO-Artemis	2023.07.25	$p(t^2)+p(y)+p(a)$	
$I+z$	SNO-Artemis	2023.07.27	$p(t)$	partial transit
$I+z$	SNO-Artemis	2023.07.28	$p(t^4)$	
z'	SNO-Artemis	2023.08.02	$p(t^3)$	
z'	SNO-Artemis	2023.08.04	$p(t^4)$	
z'	SNO-Artemis	2023.08.05	$p(t^2)$	
$I+z$	SNO-Artemis	2023.08.07	$p(t^3)+p(x^2)$	
i'	SNO-Artemis	2023.08.09	$p(t^2)+p(x)$	
$I+z$	SNO-Artemis	2023.08.14	$p(t^3)+p(x)+p(y^2)+p(f)+p(a)$	
i'	SNO-Artemis	2023.08.15	$p(t^3)$	
z'	SSO-Callisto	2023.08.22	$p(t^2)+p(y)$	
i'	SSO-Europa	2023.08.22	$p(t^2)+p(f)$	
z'	SSO-Callisto	2023.08.27	$p(t^2)+p(f)+p(a^2)$	
z'	SSO-Io	2023.08.27	$p(t^4)$	
i'	SSO-Europa	2023.08.27	$p(t)$	
i'	SSO-Ganymede	2023.08.27	$p(t^2)+p(b)$	
Ks	UKIRT/WFCAM	2023.08.27	$p(t^3)+p(x^3)+p(y)+p(f^2)+p(b^2)$	
Ks	UKIRT/WFCAM	2023.08.30	$p(t)+p(x)+p(f^2)$	
$I+z$	SSO-Callisto	2023.09.09	$p(t)+p(y^2)$	
i'	SNO-Artemis	2023.09.12	$p(t)+p(x)+p(y^2)$	
$I+z$	SSO-Io	2023.09.14	$p(t^2)$	
$I+z$	SNO-Artemis	2023.09.15	$p(t^2)$	flare
g'	MuSCAT3-2m0	2023.09.17	$p(t^2+f^2)$	15
$I+z$	SSO-Europa	2023.09.17*	$p(t^4)+p(b)$	
r'	MuSCAT3	2023.09.17	$p(t^2)+p(f)$	
i'	MuSCAT3	2023.09.17	$p(t^2)+p(f)+p(a^2)+p(b)$	
z'	MuSCAT3	2023.09.17	$p(t^4)+p(y^2)+p(f^3)$	
g'	GTC/HiPERCAM	2023.09.17	$p(t^3)$	flare
r'	GTC/HiPERCAM	2023.09.17	$p(t^3)$	flare
i'	GTC/HiPERCAM	2023.09.17	$p(t^2)+p(b)$	
z'	GTC/HiPERCAM	2023.09.17	$p(t^2)+p(x)+p(b)$	
g'	MuSCAT3-2m0	2023.09.19	$p(t^2)$	19
r'	MuSCAT3	2023.09.19	$p(t^2)+p(f^3)+p(a)$	
i'	MuSCAT3	2023.09.19	$p(t^2)+p(y)$	
z'	MuSCAT3	2023.09.19	$p(t^2)+p(x)$	
u'	GTC/HIPERCAM	2023.09.17	$p(t^4)$	flare, 33
I	T150 Sierra Nevada Observatory	2023.09.20*	$p(t^3)$	
$I+z$	SNO-Artemis	2023.09.20*	$p(t^3)$	flare
$I+z$	SNO-Artemis	2023.09.25*	$p(t^2)+p(y)+p(b)$	
$I+z$	SNO-Artemis	2023.09.27*	$p(t^2)$	
$I+z$	SNO-Artemis	2023.09.30*	$p(t^2)+p(b)$	

Supplementary Information Table 1 | SPECULOOS-3 b transit light curves used in this work. For each light curve, the selected baseline model is shown as a polynomial $p()$ of one or several external parameters, with t = time, x and y = x- and y-positions of the stellar image on the detector, f = full-width at half maximum of the stellar image, a = airmass, and b = background. * not included in the global MCMC analysis. The light curves for which the dates are followed by an asterisk were not used in the global MCMC analyses.

Filter	a	b
u'	1.168 ± 0.086	-0.194 ± 0.090
g'	1.203 ± 0.066	-0.209 ± 0.069
r'	1.027 ± 0.012	-0.113 ± 0.017
i'	0.704 ± 0.094	0.257 ± 0.085
z'	0.438 ± 0.058	0.450 ± 0.034
$I + z$	0.57 ± 0.11	0.354 ± 0.092
Ks	0.149 ± 0.017	0.373 ± 0.003

Supplementary Information Table 2 | SPECULOOS-3 limb-darkening coefficients. These coefficients were interpolated from the tables of ref. [98]. The means of the values for the i' and z' filters were adopted for the non-standard I+z filter. The errors are the 1-σ errors as derived from propagating the 1-σ errors on the stellar atmospheric parameters.

Epoch	Mid-transit timing (BJD_{TDB})	Telescope(s) + filter(s)
-510	2459423.8288 ± 0.0022	SAINT-EX, $I+z$
-507	2459425.9856 ± 0.0019	SAINT-EX, $I+z$
0	2459790.58366 ± 0.00036	SNO-Artemis, $I+z$
499	2460149.42662 ± 0.00033	SNO-Artemis, $I+z$
502	2460151.58509 ± 0.00049	SNO-Artemis, $I+z$
505	2460153.74128 ± 0.00074	SNO-Artemis, $I+z$
506	2460154.46060 ± 0.00052	SNO-Artemis, $I+z$
513	2460159.49556 ± 0.00054	SNO-Artemis, z'
516	2460161.65225 ± 0.00086	SNO-Artemis, z'
517	2460162.37136 ± 0.00060	SNO-Artemis, z'
520	2460164.52913 ± 0.00080	SNO-Artemis, $I+z$
523	2460166.6858 ± 0.0011	SNO-Artemis, i'
530	2460171.72027 ± 0.00032	SNO-Artemis, $I+z$
531	2460172.43941 ± 0.00051	SNO-Artemis, i'
541	2460179.63018 ± 0.00054	SSO-Callisto, z'; SSO-Europa, i'
547	2460183.94485 ± 0.00091	UKIRT/WFCAM, Ks
548	2460184.66468 ± 0.00032	SSO-Callisto+Io , z'
		SSO-Europa+Ganymede, i'
551	2460186.82161 ± 0.00026	UKIRT/WFCAM, Ks
566	2460197.60841 ± 0.00061	SSO-Callisto, $I+z$
570	2460200.48547 ± 0.00076	SNO-Artemis, i'
573	2460202.64323 ± 0.00097	SSO-Io, i'
574	2460203.36185 ± 0.00067	SNO-Artemis, $I+z$
576	2460204.80016 ± 0.00031	MuSCAT3, r', i', z'
		SSO-Io, $I+z$
577	2460205.519183 ± 0.000066	GTC/HiPERCAM, g', r', i', z'
579	2460206.95793 ± 0.00054	MuSCAT3, r', i', z'
581	2460208.39517 ± 0.00026	SNO-Artemis, $I+z$
		T150 Sierra Nevada I
588	2460213.42988 ± 0.00048	SNO-Artemis, $I+z$
591	2460215.5883 ± 0.0012	SNO-Artemis, $I+z$
595	2460218.46361 ± 0.00043	SNO-Artemis, $I+z$

Supplementary Information Table 3 | SPECULOOS-3 b mid-transit timings. The values and errors are the mean and standard deviation of the posterior probability distributions derived from an MCMC analysis.